

## $\gamma^2$ VELORUM: COMBINING INTERFEROMETRIC OBSERVATIONS WITH HYDRODYNAMIC SIMULATIONS

A. Lamberts<sup>1</sup> and F. Millour<sup>2</sup>

**Abstract.** Colliding stellar winds in massive binary systems have been studied through their radio and strong X-ray emission for decades. More recently, spectro-interferometric observations in the near infrared have become available for certain binaries, but identifying the different contributions to the emission remains a challenge. Multidimensional hydrodynamic simulations reveal a complex double shocked structure and can guide the analysis of observational data. In this work, we analyse the wind collision region in the WR+O binary,  $\gamma^2$  Velorum. We combine multi-epoch AMBER observations with mock data obtained with hydrodynamic simulations with the RAMSES code. We assess the contributions of the wind collision region in order to constrain the wind structure of both stars.

Keywords: stars:binaries:spectroscopic, stars:Wolf-Rayet, stars:winds, outflows, techniques:interferometric, methods:numerical, stars:individual: $\gamma^2$  Velorum

### 1 Introduction

The strong photon field of massive stars enables them to drive supersonic winds ( $v \simeq 1000 - 3000 \text{ km s}^{-1}$ ) with mass loss rates varying from  $10^{-8} M_{\odot} \text{ yr}^{-1}$  for O stars to  $10^{-5} M_{\odot} \text{ yr}^{-1}$  for Wolf-Rayet (WR) stars. These winds are a crucial aspect to the evolution of massive stars. They also impact their surrounding medium, by the injection of momentum and metals during the final stages. Colliding wind binaries provide a unique opportunity to probe the structure of stellar winds. The interaction of both winds creates a warm and dense shocked region, with strong X-ray emission (Stevens et al. 1992). The geometry of the shock cone can be inferred from phase-locked variability in UV, optical and IR emission lines, as well as non-thermal radio-observations in certain systems. As such colliding wind binaries provide much more observables than isolated systems and provide crucial information on stellar winds.

$\gamma^2$  Velorum is the closest known WR+O binary and is an ideal target for in depth study of the colliding wind region (St.-Louis et al. 1993; Willis et al. 1995; Henley et al. 2005). Detailed modelling of the of the optical and infrared spectra (De Marco & Schmutz 1999; De Marco et al. 2000) allows to determine most of the stellar and wind parameters for both stars, but direct observation of the O-star remains a challenge, as it is strongly embedded in the wind collision zone. Infrared interferometry offers a unique opportunity to put constraints on the spatial extension of the wind collision zone and its relative flux. Previous work (Millour et al. 2007) based on AMBER observations refined the spectral types of the stars and highlighted the presence of strong residuals in the data but was unable to attribute them to the wind collision region.

In this work, we present a direct comparison of interferometric data and mock data from hydrodynamic simulations. The 3D simulations present an accurate model of the temperature and density in the wind collision region, from which we can derive the corresponding emitted flux. The resulting extended emission is well matched by the data. This work is the first identification of a wind collision region with interferometric data in the infrared.

---

<sup>1</sup> Department of Physics, University of Wisconsin-Milwaukee, 3135 N. Maryland Avenue, Milwaukee, WI 53211, USA

<sup>2</sup> Laboratoire Lagrange, UMR 7293 UNS-CNRS OCA, Boulevard de l'Observatoire, B.P. 4229 F, 06304 Nice Cedex 4, France

## 2 Combining interferometric data and hydrodynamic simulations

### 2.1 Observations and data analysis

We use interferometric data obtained with AMBER (Astronomical Multi-BEam Recombiner (Petrov et al. 2007)) on the Very Large Telescope Interferometer (VLTI). AMBER provides spectra in the J,H and K bands, with a maximal resolution of  $\Delta\lambda/\lambda = 12000$ . While multiple observations from 2004 until 2012 provide a good coverage of the 79d orbital period, the work we present here focuses on the orbital phase  $\phi \simeq 0.8$ , where the binary is in the plane of the sky. Using the `fitOmatic` software (developed in house, see Millour et al. (2009)), we isolate two different spectra. The first one is clearly associated with the luminous WR star, while the second one is spatially associated with the region around the O-star. As such, it probably includes features from the O-star wind and the WR star wind but also the wind collision region. This is suggested by the presence of important residuals when subtracting the WR spectrum from the O-star spectrum.

While detailed modeling of the spectral lines is beyond the scope of our work we use hydrodynamic simulations to reproduce the continuum emission and derive visibility curves.

### 2.2 Numerical simulations and mock data

We use the RAMSES code (Teyssier 2002) to solve the equations of hydrodynamics in three dimensions. The code is based on a second order Godunov method on a Cartesian grid. It allows for adaptive mesh refinement (AMR), meaning that the resolution can be locally increased according to the properties of the flow. It is perfectly suited for the study of colliding wind binaries, where refinement according to density gradients will naturally enhance the resolution around the shocks (see e.g. Lamberts et al. (2011)).

The winds are generated in two spherical regions, which are reset at each timestep. The winds are spherical and are launched with their terminal velocity. We include orbital motion of the stars and radiative cooling in the shocked region. We model a region covering six times the binary separation. The amount of flux in the shocked region outside of our simulation domain is negligible. We use the wind and stellar parameters derived in De Marco et al. (2000) and the orbital parameters from Schmutz et al. (1997).

Figure 1 shows the density, velocity and temperature in the orbital plane for the orbital phase  $\phi = 0.8$ . The temperature map clearly highlights the warm shocked region. At the apex, the wind velocity is very low but then increases up to supersonic values further out. Both shocked winds are separated by a contact discontinuity, as can be seen on the density map. Due to the lower density, the O-star wind is less subject to radiative cooling and has a temperature of more than  $10^8$  K at the apex of the shock. The WR wind on the other hand cools down to about  $10^7$  K in the whole shocked region. The shocked region presents a limited development of both the Kelvin-Helmholtz and the non-linear thin shell instability (Vishniac 1994), which should not be sufficient to yield any temporal variability in the system.

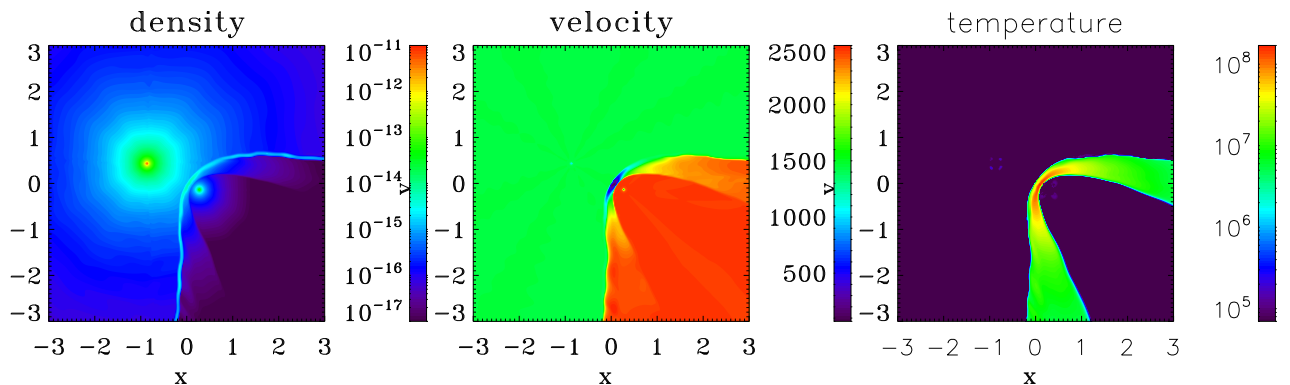


**Fig. 1.** Density ( $\text{g cm}^{-3}$ ), velocity ( $\text{km s}^{-1}$ ) and temperature (K) in the orbital plane of  $\gamma^2$  Vel at  $\phi = 0.8$ . The lengthscale is given in units of the binary separation. The WR star is on the top left, the O star on the bottom right.

To compare with the emission from the unshocked winds, we compute the free-free emission from the wind collision region only. First, we compute the emissivity in all shocked cells (those with  $T \geq 10^5$  K) and then

we take into account the absorption along the line of sight. As we included a passive scalar in the simulation, we can distinguish both winds and account for the chemical enrichment of the WR wind. The emission of the WR wind is determined by a model derived from Dessart et al. (2000) and the O star is considered as a point source (i.e. the contribution of its free wind is neglected). Figure 2 shows the resulting emission map at  $2\mu m$ . The map shows extended emission from the shocked region. At this stage, we have not determined the exact impact on the emitted spectra.

However, we have assessed the contribution of this extended source on the visibility of the system. The visibility is an interferometric measurement related to the spatial extension of a source. A low visibility indicates an extended emitting region. The left panel of figure 3 shows the observed visibility curve in  $\gamma^2$  Vel (in red) as well as a mock curve (in black) based on a model including the emission from both stars and the Wolf-Rayet wind, but no wind collision region. The model does not match the data, indicating an extended source contributes to the emission. The right panel shows mock visibility curves extracted from the simulation. Again, the black curves assumes the wind collision region does not contribute to the emission. The green and red curves assume an arbitrary contribution of 2.5% and 5% of the total flux respectively. While the quantitative analysis is still in progress, these plots show that the wind collision region impact the total emission and can be detected with infrared interferometry.

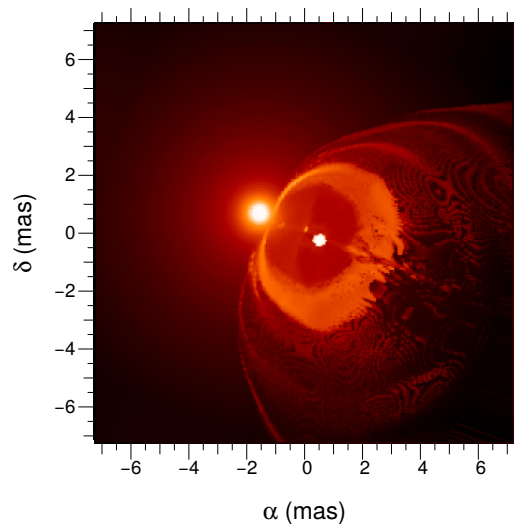


**Fig. 2.** Flux at  $2\mu$  at  $\phi = 0.8$ . The color scale is arbitrary and logarithmic.

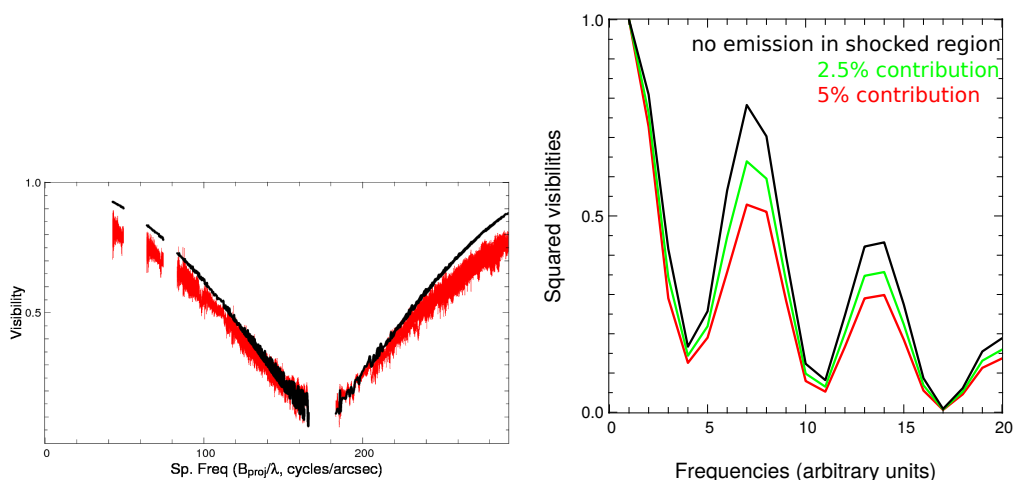


**Fig. 3.** Left: Observed (red) and mock visibility curve, assuming two stars without wind collision region. Right: Visibility curves with different respective contributions, based on the numerical simulation.

### 3 Looking further

In this work we confirm the first detection of a wind collision region with infrared interferometry. Although  $\gamma^2$  Vel is an ideal target for such observations, the identification of the wind collision region is not straightforward, due to the complex geometry of the system. Therefore, we have performed three-dimensional hydrodynamic simulations to model the structure of the system and determine its continuum emission. The resulting emission map shows that the wind collision region displays extended emission and decreases the visibility curve of the system. Our preliminary qualitative analysis matches the data and allows us to confirm the detection of the wind collision region. Further work will include more quantitative results including several orbital phases.

**Acknowledgments:** This work was initiated by Olivier Chesneau, who passed away before seeing the confirmation of the detection. We thank him for his insight to start this collaboration between observation and theory. Astrid Lamberts is supported by the UWM Research Growth Initiative, the NASA ATP program through NASA grant NNX13AH43G, and NSF grant AST-1255469. Simulations were performed at the NASA Advanced Supercomputing Division.

### References

- De Marco, O. & Schmutz, W. 1999, *A&A*, 345, 163  
De Marco, O., Schmutz, W., Crowther, P. A., et al. 2000, *A&A*, 358, 187  
Dessart, L., Crowther, P. A., Hillier, D. J., et al. 2000, *MNRAS*, 315, 407  
Henley, D. B., Stevens, I. R., & Pittard, J. M. 2005, *MNRAS*, 356, 1308  
Lamberts, A., Fromang, S., & Dubus, G. 2011, *MNRAS*, 418, 2618  
Millour, F., Chesneau, O., Borges Fernandes, M., et al. 2009, *A&A*, 507, 317  
Millour, F., Petrov, R. G., Chesneau, O., et al. 2007, *A&A*, 464, 107  
Petrov, R. G., Malbet, F., Weigelt, G., et al. 2007, *A&A*, 464, 1  
Schmutz, W., Schweickhardt, J., Stahl, O., et al. 1997, *A&A*, 328, 219  
St.-Louis, N., Willis, A. J., & Stevens, I. R. 1993, *ApJ*, 415, 298  
Stevens, I. R., Blondin, J. M., & Pollock, A. M. T. 1992, *ApJ*, 386, 265  
Teyssier, R. 2002, *A&A*, 385, 337  
Vishniac, E. T. 1994, *ApJ*, 428, 186  
Willis, A. J., Schild, H., & Stevens, I. R. 1995, *A&A*, 298, 549